JOURNAL OF GEOPHYSICAL RESEARCH, VOL. 115, A12214, doi:10.1029/2010JA015931, 2010

Automatic Whistler Detector and Analyzer system: Implementation of the analyzer algorithm

János Lichtenberger,[1] Csaba Ferencz,[1] Daniel Hamar,[1] Peter Steinbach,[2] Craig J. Rodger,[3] Mark A. Clilverd,[4] and Andrew B. Collier[5,6]

Received 14 July 2010; revised 13 October 2010; accepted 22 October 2010; published 7 December 2010.

[1] The full potential of whistlers for monitoring plasmaspheric electron density variations has not yet been realized. The primary reason is the vast human effort required for the analysis of whistler traces. Recently, the first part of a complete whistler analysis procedure was successfully automated, i.e., the automatic detection of whistler traces from the raw broadband VLF signal was achieved. This study describes a new algorithm developed to determine plasmaspheric electron density measurements from whistler traces, based on a Virtual (Whistler) Trace Transformation, using a 2-D fast Fourier transform transformation. This algorithm can be automated and can thus form the final step to complete an Automatic Whistler Detector and Analyzer (AWDA) system. In this second AWDA paper, the practical implementation of the Automatic Whistler Analyzer (AWA) algorithm is discussed and a feasible solution is presented. The practical implementation of the algorithm is able to track the variations of plasmasphere in quasi real time on a PC cluster with 100 CPU cores. The electron densities obtained by the AWA method can be used in investigations such as plasmasphere dynamics, ionosphere-plasmasphere coupling, or in space weather models.

Citation: Lichtenberger, J., C. Ferencz, D. Hamar, P. Steinbach, C. J. Rodger, M. A. Clilverd, and A. B. Collier (2010), Automatic Whistler Detector and Analyzer system: Implementation of the analyzer algorithm, *J. Geophys. Res.*, *115*, A12214, doi:10.1029/2010JA015931.

1. Introduction

[2] All space weather models and forecasting methods are dependent on data for either boundary conditions or the specification of model parameters. At best these data come from in situ observations or a statistical model parameterized by geomagnetic indices. In the worst case estimates are used to provide some representative values. In situ satellite observations are able to measure the densities directly and can sample wide and continuous latitudinal and longitudinal ranges, but suffer from a number of inherent weaknesses: very few platforms give simultaneous comprehensive measurements of particles, waves and fields. Data availability is also very often limited in space and time: at best there will be a handful of observations of a given parameter at any given time throughout all of geospace. With very few exceptions (such as GOES data), data are generally not available in real or even near-real time, limiting their use for forecasting. Finally, the high costs of satellite fabrication and launch make it unlikely that these limitations will be overcome any time soon. However, ground based measurements provide a complementary or alternative data source for space weather models. Clearly the combination of ground and space based measurements would provide the best results, but the ground based measurements have several advantages over the space based ones. They are generally inexpensive and can produce continuous temporal and spatial coverage, which may be limited by the occurrence of the phenomena. Most ground-based stations have access to the Internet, thus capable of providing real-time data.

[3] *Reeves* [1998] found that geomagnetic storms produce all possible responses in the outer belt relativistic electron flux levels at geostationary orbits, i.e., flux increases (53%), flux decreases (19%), and no change (28%). The dynamics of these flux variations are the result of a complex interplay of acceleration, loss and transport processes. For all of these processes the underlying mechanism has a strong dependence on the distribution of the overlapping background cold plasma in the plasmasphere. Acceleration and loss are due to resonances with a variety of plasma waves. Both the generation of these waves and the resulting resonance conditions depend on mass loading of field lines and thus also on the ambient plasma density [*Horne and Thorne*, 2003; *Horne et al.*, 2007; *Meredith et al.*, 2007].

[4] The cold electron density distribution of the plasmasphere is a key parameter for modeling the plasmasphere and radiation belts, but is difficult to measure routinely. Whistlers have been regarded as cheap and effective tools for case

[1]Space Research Group, Department of Geophysics and Space Sciences, Eötvös University, Budapest, Hungary.
[2]Research Group for Geology, Geophysics and Space Sciences, Hungarian Academy of Sciences, Budapest, Hungary.
[3]Department of Physics, University of Otago, Dunedin, New Zealand.
[4]British Antarctic Survey, Cambridge, UK.
[5]Hermanus Magnetic Observatory, Hermanus, South Africa.
[6]School of Physics, University of KwaZulu-Natal, Durban, South Africa.

0148-0227/10/2010JA015931

studies of plasmasphere diagnostics since the early years of whistler research [*Storey*, 1953], but have not been used as an operational tool since reducing whistler data to equatorial densities is very labor intensive for statistical studies. These equatorial densities were obtained by whistler inversion analysis, which in turn was based on a combination of wave propagation, plasmaspheric electron density distribution and magnetic field models. Such equatorial electron number density measurements based on operator-scaled whistler data led to the discovery of the plasmapause [*Carpenter*, 1963]. The first, widely used, coherent whistler inversion method for nose whistlers was developed by *Park* [1972], which was extended to low- and mid-latitude whistlers by *Tarcsai* [1975] based on the nose extension method of *Bernard* [1973]. Numerous studies have been presented which use whistlers to explore the dynamics of the plasmasphere [e.g., *Park*, 1974; *Tarcsai et al.*, 1988; *Carpenter*, 1988; *Carpenter et al.*, 1993] and to build equatorial electron density models of the plasmasphere [*Carpenter and Anderson*, 1992]. However, all of these studies relied upon manual analysis of whistler data. Broadband VLF recordings extending over a few decades probably contain millions of whistlers that can be used in plasmasphere diagnostic studies. The recently developed Automatic Whistler Detector system setup at various AWDANet nodes [*Lichtenberger et al.*, 2008] collects whistlers in high numbers, e.g., the rate at the Antarctic peninsula is close to 10 million per year. However, the human effort needed to analyze a whistler is rather on the order of an hour than a minute, (this estimate is based on long-term experiences of many researchers) thus this huge potential cannot be utilized fully this way. In this study we describe an algorithm that can overcome this bottleneck and can be used to automate the whistler analysis procedure.

2. Automatic Whistler Analyzer Algorithm

[5] Traditional whistler inversion methods are based on "scaled" whistlers [*Park*, 1972; *Tarcsai*, 1975; *Sazhin et al.*, 1992]. Scaling in this context means reading the frequency-time coordinates of a whistler trace on a frequency-time diagram (spectrogram). Then these coordinates are used exclusively as an input for the inversion method. Therefore the obvious and natural way to automate the analysis would be to automate the scaling itself, because the remaining task is simply applying the inversion method to the input data. A computer algorithm based on an enhanced Park method has been available for decades [*Tarcsai*, 1975]. Machine reading of frequency-time pairs is easy and straightforward in the case of a model whistler, where there are no noise sources and the whistler trace appears as a continuous, solid curve on the spectrogram. However, developing and implementing a machine-scaling algorithm for naturally occurring whistlers has proved to be unsuccessful until now. The identification and scaling of a whistler trace are simple tasks for a human, but very difficult for a computer algorithm because the whistler recorded at a ground station is always contaminated by additional signals, such as sferics, VLF transmitter broadcasts, power line harmonics and other local noise. Beside these sources of additional signals, the whistler signal arriving at the receiver is usually not a clean gliding tone, but a compound signal resulting from interference which occurred at the source of the signal and during the propagation (including the subionospheric, ionospheric and magnetospheric) paths [*Strangeways*, 1982; *Hamar et al.*, 1992]. Thus the whistler trace on a spectrogram is never a solid hyperbolic line (which would make automatic analysis easy), but rather appears as distinct patches with smaller or larger gaps between them, an example of which can be seen in Figure 2a, where the last (rightmost) trace is not a solid line, but built up of distinct patches each with a different power. These whistler patches overlap with the patches produced by the additional signals discussed above. We have tried to adopt and apply various signal and image processing methods developed for similar machine reading problems, e.g., approaches that were attempted and subsequently rejected included ridge detection and the technique applied for ionograms. They were used in combination with information regarding the propagation of a whistler. The best results obtained produced frequency-time pairs only for small sections of whistler traces which cannot be used for proper inversion.

[6] However, the virtual (whistler) trace transformation (VTT) introduced recently by *Lichtenberger* [2009] based on recent advances in wave propagation [*Ferencz et al.*, 2001] and field-aligned electron density distribution models [*Denton et al.*, 2002] uses a different approach. Here the technique can be applied not only for a set of scaled frequency-time points, but to the spectrogram directly. It uses a fourth assumption besides the wave propagation, field-aligned electron density distribution and magnetic field models: a simplified model of equatorial electron density distribution. The inversion process for whistlers depends on the epoch time of source lightning, dt, the equatorial electron density, $n_{eq}(L)$, and L value, while the VTT based on this extended model depends on dt and two parameters, A and B, describing the exponential decrease of plasmaspheric electron density in the equatorial plane [*Lichtenberger*, 2009, equation (8)]:

$$\log_{10} n_{eq} = A + BL, 1.4 < L < 8. \quad (1)$$

If one assumes a priori knowledge of these three parameters then applying a VTT to a spectrogram of a multiple path (MP) whistler group (whistlers with two or more components, each of which was generated by the same lightning stroke but traversed a different path through the plasmasphere), will generate a transformed matrix that will render the hyperbolic curves of whistler traces into straight, vertical structures (in the case of noise-free model whistlers, these would be solid, vertical lines). If the three parameters of the VTT do not match the real propagation parameters of this MP whistler group, the result will be a nonvertical and/or nonstraight structure. Though the VTT was introduced to transform MP whistler groups (in this case the A and B parameters of the VTT will describe the electron density variation in the L range covered by the MP whistler group and provide a good estimate outside of this range), it works equally well for a single whistler trace in a mathematical sense. However in this case it provides the electron density only for a single L shell. If there are two or more close or overlapping MP whistler groups on a spectrogram, e.g., two MP whistler groups that propagated on the same paths and were generated by two consecutive lightning strokes, VTT will transform only one group into a straight, vertical structure, because the excitation times are

different. Thus, with the introduction of VTT, the problem of machine reading of a spectrogram (and thus the scaling of the whistler traces) is transformed into the problem of the identification of verticality and straightness of structures in a 2-D matrix.

[7] The 2-D Fourier transform (which is a 2-D fast Fourier transform (FFT) in practical implementations) has the following known features: it transforms a vertical line into a horizontal line and vice versa, while a sloping straight line is transformed into another straight line but with different slope. Figures 1a, 1b, 1c, and 1d show an example of combining VTT with 2-D FFT applied to a modeled MP whistler group. Figure 1a shows the spectrogram of a model MP whistler group, Figure 1b shows the output of the VTT, while the 2-D FFT of output of the VTT is in Figure 1c. The vertical lines are now transformed into a horizontal line at zero frequency. The "broadening" of the lower-frequency section of the transformed traces are due to the finite resolution of the spectrogram and because the horizontal thickness of the traces is broader at low frequencies, a point on VTT image is generated by shifting it horizontally, mapping an (f_i, t_i) point to (f_i, t_n) point, t_n is the time of arrival of the nose frequency. This is also visible in the 2-D FFT image, as the vertical lobe structure at the center of the image. Figure 1d shows the sum of the absolute values of the 2-D FFT matrix elements along the lines drawn through the center of the 2-D FFT matrix as a function of inclination with 0.1° steps. Note that the 0° value here corresponds to the sum calculated along the vertical line. This plot represents the spread of lines, the sharper the line, the narrower the curve near the peak, which can be called a "sharpness plot" in this context. In this plot, three independent numbers can be identified (1) the peak value, $p_{\max}$, of the curve, (2) the location (angle), α, of the peak, and (3) the sharpness of the peak, w, which can be the full width at half maximum (FWHM). This can be better seen in Figures 1e, 1f, 1g, and 1h, where the case of two MP groups propagating on the same path but generated by two consecutive lightning strokes is modeled. The nonstraight and nonvertical structures appear on 2-D FFT image as "rays" crossing the center of the image (Figure 1g) and as local maxima on sharpness plot (Figure 1h). Thus the existence of such maxima can be used as an indication of overlapping groups.

[8] Figure 2 has structures similar to those seen in Figure 1, but it shows the modeling output for two real MP whistler groups. This clearly illustrates the advantages of the 2-D Fourier transform as well as the usefulness of the sharpness plot. The image in the Figure 2b shows the VTT image created by applying VTT to a simplified spectrogram matrix having only 10000 nonzero elements, enhancing the whistler traces and suppressing a majority of the other features. This simplified spectrogram is created by using a reassigned spectrogram [*Kodera et al.*, 1976; *Flandrin*, 1999] instead of the standard spectrogram based on short time (window) FFT. The unwanted features in the reassigned spectrogram are removed by using stationary phase in the complex reassigned spectrogram matrix, that is selecting those signals (matrix elements), where the phase is slowly varying from one element to the other, this removes the nondeterministic, noise like signals and by calculating $S_h = \Sigma_i R_{ij}$ and $S_v = \Sigma_j R_{ij}$ from the reassigned spectrogram matrix R. The sferics are removed by applying a threshold to S_v, the power line harmonics and VLF transmitters are removed by thresholding S_h.

[9] A thorough investigation of the result of VTT in Figures 2e, 2f, 2g, and 2h shows that not two, but rather three superimposed whistler groups are in this recording, though the third one is weaker than the first two. There are three groups of near-vertical structures, the first group contains vertical structures, the second group consists of structures slanting to the left (mainly in the left part of Figure 2f, labeled as "2"), while in the third group (located in the right half of Figure 2f, labeled as "3") the structures are slanting to the right.

[10] These plots demonstrate the solution for the automated whistler analyzer algorithm, which consists of the following steps:

[11] 1. Application of VTT to the spectrogram matrix with an initial set of (dt, A, B) parameter triplet.

[12] 2. Computation of 2-D FFT of VTT image.

[13] 3. Calculation of sharpness plot for the 2-D FFT image and $p_{\max}$, $|\alpha - 90|$ and w from it. The sharpness plot is used as an input into the objective function in the optimization procedure, but instead of the usual construction of the residual vector from the estimated and measured objective function values, a "logical" residual vector is constructed from the above mentioned criteria for the three parameters. The elements of this vector are the logical values of the three estimated parameters ($p_{\max}$,$|\alpha - 90|$, w) status with respect to the previous iteration: ($L_{p\max}$, $L_{|\alpha-90|}$, Lw), where L_i is either "True" or "False". True if $-p_{\max}$ is smaller and False if it is bigger, the same is true in the case of w and $|\alpha - 90|$. The construction of a standard residual vector is not feasible, since it would require the comparison of the sharpness plot calculated for a model whistler group with the one derived from measured data. In order to accomplish this, the L value of the propagation for the traces would have to be known in advance. Therefore three cross-coupled, modified simplex methods (separate ones for optimizing $-p_{\max}$, $|\alpha - 90|$ and w) are used for optimization, where the logical residual vector with weighting factors is used to couple the parallel processes: first, in the nth iteration, the objective function values in the three parallel simplex method procedures and also the relative difference to the ones obtained during the previous iteration are calculated, e.g., for w it is $\Delta w = (w_n - w_{n-1})/w_{n-1}$. Then a modified w^* is calculated using these differences as weighting factors

$$w^* = w\, s\left(L_{p_{\max}}\right)(1 + \Delta p_{\max})\; s\left(L_{|\alpha-90|}\right)(1 + \Delta|\alpha - 90|), \quad (2)$$

where $s(L_i)$ is + 1 if L_i = True and −1 if L_i = False, L_i is the ith element of the logical residual vector and i = 1, 2 in this case. The modified values of $p^*_{\max}$ and $|\alpha - 90|^*$ are calculated in the same way, using the corresponding relative differences and elements from the logical residual vector. Instead of the standard objective function values, the modified ones are passed to the simplex procedures to continue with.

[14] 4. Iterate steps 1–3 while tuning the (dt, A, B) triplet to simultaneously maximize $p_{\max}$ while minimizing $|\alpha - 90|$ and w.

[15] The verification of this algorithm has been done on several sets of processed MP groups mentioned by *Lichtenberger* [2009]. The verification showed that the extremum values of $p_{\max}$, $|\alpha - 90|$ and w derived from the algorithm correspond to the visually proved best vertical of VTTs. We have analyzed 78 MP groups manually (adjusting

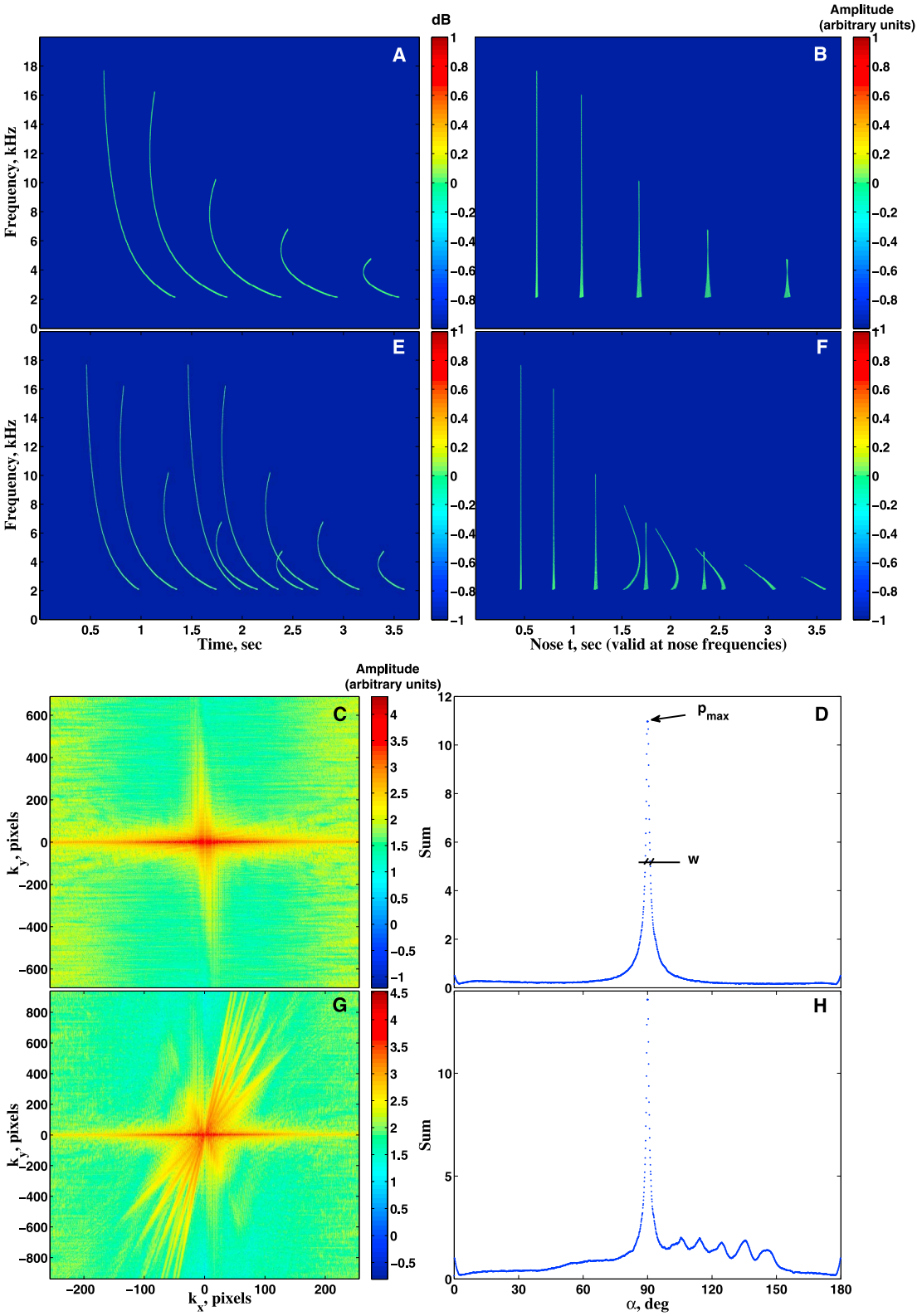

Figure 1. The principles of AWA algorithm. A model MP whistler group (Figures 1a, 1b, 1c, and 1d) and an overlapping model MP whistler group (Figures 1e, 1f, 1g, and 1h). (a and e) Spectrogram of the whistler group, (b and f) VTT of the whistler group in Figures 1a and 1e, (c and g) 2-D FFT image (absolute value) of VTT matrix, and (d and h) sum of the 2-D FFT image along the lines drawn through the center of the image, in arbitrary units. The sums were calculated up to 256 points from the center of the image in all directions. Note that α is measured from vertical. The color bars are scaled in arbitrary units. The Y axes of Figures 1b and 1f are the same as those in Figures 1a and 1e.

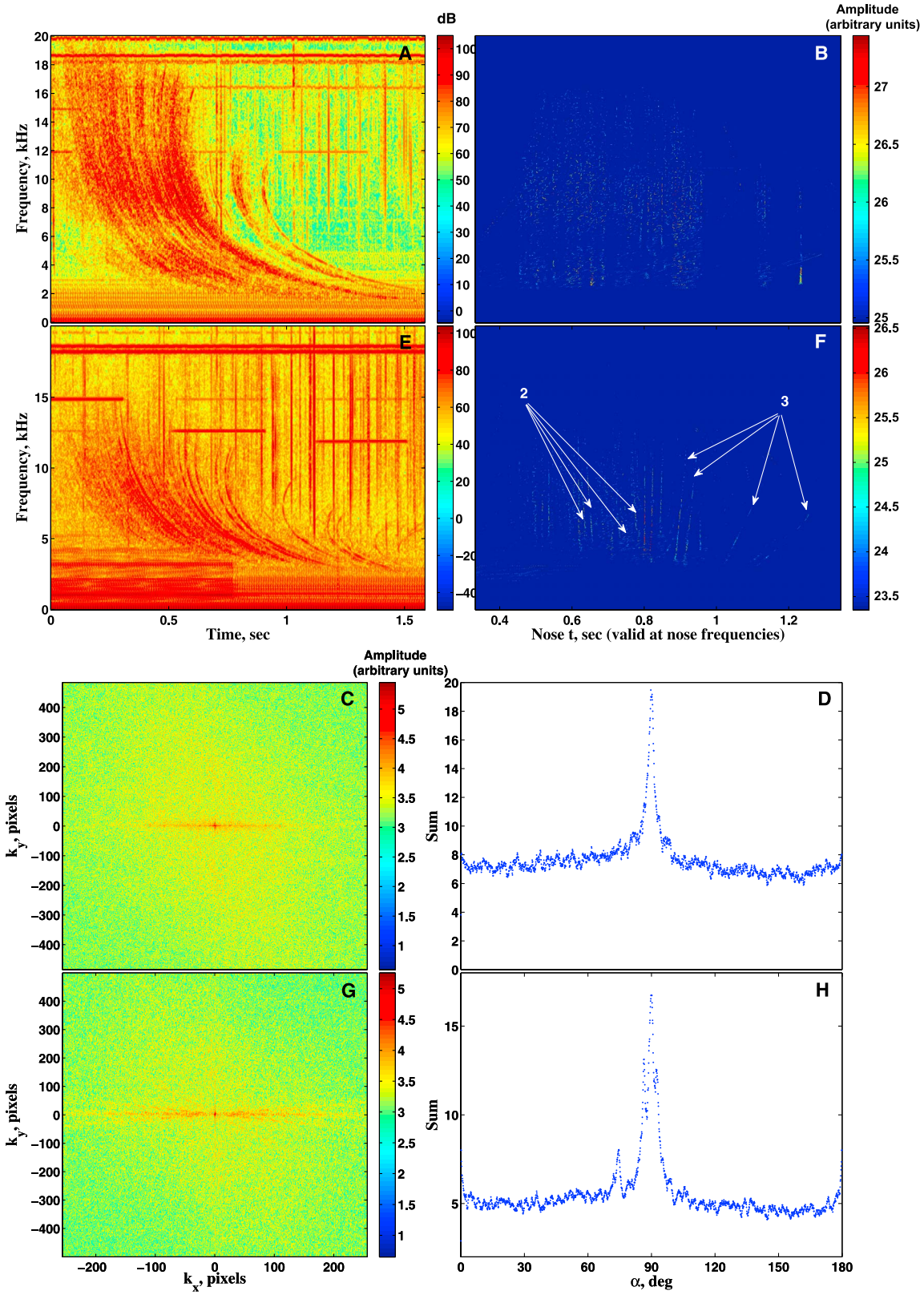

Figure 2. Same as Figure 1 but applied to naturally occurring whistlers. (a, b, c, and d) A MP whistler group recorded in Dunedin, New Zealand at 1150:23 UT on 4 February 2006 and (e, f, g, and h) a whistler recording exhibiting overlapping MP groups, recorded in Dunedin, New Zealand at 0430:50 UT on 23 July 2007. Figures 2b and 2f showing VTT matrix that are very difficult to visualize, because VTT matrix is almost empty (there are 10,000 nonzero elements in the 1024 × 1600 matrix).The best view can be achieved by zooming it up to at least 150% on a computer screen. See text for details.

Table 1. Comparison of the Results of AWA With Manual Processing on MP Groups[a]

Number of MP Groups Analyzed	$\Delta p < 5\%$	$\Delta p > 5\%$	Number of Failed Runs
78	59	4	15

[a]See text for details.

(dt, A, B) while watching the VTT image) and compared the obtained parameters with the results of Automatic Whistler Analyzer (AWA) runs on the same set. Table 1 shows the results, the number of cases when the relative differences between the two parameter sets is less than 5%, the same but for the cases when this difference is larger than 5%, and the number of cases when the AWA run failed (no convergent solution achieved). $\Delta p = (p_{AWA} - p_{manual})/p_{manual}$, where p is either dt, A or B, whichever is greatest. In the case of the "$\Delta p < 5\%$" column, all the three relative differences were smaller than 5%, while in the case of the "$\Delta p > 5\%$" column at least one of the 3 relative differences was larger than 5%. However, the relative performance of AWA with respect to the manual analysis is not relevant, because only a fraction of detected whistler events will be analyzed by AWA (see section 3 for details) and the result of AWA on a whistler group has to be qualified alone. Therefore we define two separate thresholds, beyond which the output of the optimization procedure is rejected as invalid. The first one is a quantitative measure: $p_{\max}/\overline{S} > 2.3$, where S is the sharpness plot function and $\overline{S}$ is the mean value of S. The higher this ratio, the larger the number of points which have been rendered into vertical structure. This 2.3 threshold is based on the analysis of the 78 groups presented in Table 1. If $p_{\max}/\overline{S} < 2.3$, the result is dropped and directed to another queue for later (incidental) manual control. The second quality measure is the value of α, it has to be $90° \pm 0.3°$ while it should be the minimum in the optimization process. Cases when $\alpha < 89.7°$ or $\alpha > 90.3°$ are also dropped and directed to another queue for later (incidental) manual control. Another quality measure is the final VTT image itself, it can of course be used by human being only, but the purpose is that the quality of the parameters can be visually checked at any later time and the actual threshold value (2.3) can be adjusted based on larger processed data set in the future.

3. Practical Implementation of Automatic Whistler Analyzer

[16] A straightforward mathematical implementation of this algorithm can be achieved through a standard multivariate optimization algorithm like the conjugate gradient method. However, the extremum values of $p_{\max}$, $|\alpha - 90|$ and w as a function of (dt, A, B) exhibit many local peaks, thus the global optimum can only be located if the initial parameter set is relatively close to the real optimum parameters. Local peaks occur for example when dt is close to the real value and A and B is unmatched, in this case the traces are transformed to sloping lines as it can be seen in Figure 7b of *Lichtenberger* [2009] and thus the sharpness function has a peak at an angle other than 90°. Similarly, if A and B are close to the real values, while dt is not, the traces form curves like those in Figures 7c and 7d of *Lichtenberger* [2009] and $p_{\max}$ exhibits a local peak. Direct search methods such as particle swarm optimization (PSO) reach the global optimum only if the number of particles are high enough. But in this case the average time required to find the optimum is 24 to 48 h on a recent CPU (single core of a Core 2 CPU with 2.8GHz clock rate). Thus the solution is to combine the direct search, that is calculation of points of extremum surface on a rough grid ("first run") to obtain a good initial set of (dt, A, B), with a standard optimization algorithm ("second run", simplex method) using this set as initial parameters. The first run on the rough grid takes 2.8 to 3.3 h, while the time for the second run varies from 0.55 to 2.8 h. Thus the average time needed for the automatic analysis of a 1 s long single MP whistler group is 4.4 to 5 h. The time needed for the automatic analysis of a single whistler event is 20–30% less, because the simplified spectrogram matrix used as an input for VTT contains fewer nonzero elements.

[17] A practical implementation of AWA has various requirements, the most important success criteria are as follows:

[18] 1. It has to operate in quasi real time, because the resulting data is to be used in real-time or near-real-time diagnostic and modeling of the plasmasphere and space weather investigations. This means, that, over the long-term, except for during very high-activity periods, the automatic analysis of traces should be completed within a given period of their time of arrival. Taking into account the potential applications, such as space weather, this period should be in the order of an hour. Long-term, in this case, could thus be a day. As discussed by *Lichtenberger et al.* [2008] a whistler trace can be either countable (a whistler trace that a trained human eye can identify) or scalable (a whistler trace that is suitable for analysis). A scalable whistler is countable, but the opposite is not necessarily true. Of the countable whistlers, 5–20% are scalable, depending on season and whistler rate. The observed (countable) whistler rate is highly variable from location to location, ranging from 100,000 traces per year (Tihany, Hungary or Dunedin, New Zealand) to 5–6 million traces per year (Rothera, Antarctica). This corresponds to 0.5–2 scalable events per hour for low-activity regions and 40–140 scalable events/hour for the highest-activity region. On the other hand, there are days at the Antarctic Peninsula when whistlers are literally observed in each second, such that 180–800 scalable events/hour are expected. In contrast the highest rate at low-activity regions is around 5000 traces per day [*Lichtenberger et al.*, 2008; *Rodger et al.*, 2009], thus the estimated scalable whistler rate is 10–40 per hour on those days. Taking into account the time scale of variations in plasmaspheric electron densities (it is on the order of hours), which can be attributed either to MLT variation at a given location or to the dynamics of plasmasphere, 10–15 snapshot observations per hour of the equatorial density with a meridional cross section is likely to be dense enough to describe significant dynamics. This means that a quasi real-time implementation should be able to complete the analysis of a MP whistler group within 250–300 s. During high-activity periods, it is only fast enough to analyze a fraction of scalable events, directing the rest into an off-line processing queue.

[19] 2. The hardware on which the AWA is implemented has to be compact in physical dimension and weight. Many systems are likely to be installed at remote locations, and there is no chance to use large, heavy equipment to transport it to the remote site.

[20] 3. Finally, the price of the hardware should fit into the generally available budgets of institutions which are involved in the study of whistlers. Of course, this is not a scientific issue, but is significant as the practical implementation of a global network of stations would require at least 10–15 stations to have optimum coverage both in (magnetic) latitude and longitude. This station number comes from considering the diurnal and seasonal variations in whistler activity. AWDANet [*Lichtenberger et al.*, 2008] is such a planned network of automatic whistler analyzers, and will require all of these criterion to be met in order to be successful. The map of existing and planned nodes of AWDANet is shown in Figures 13 and 14 of *Lichtenberger et al.* [2008].

[21] Comparing the times and frequencies in Criterion 1 with the time needed for the AWA on a single (recent) CPU, one can conclude that a factor of 100 increase in processing speed would be adequate for analyzing 10–15 whistler events per hour, that can be achieved by a cluster built of 12–15 PCs with quad core/eight thread CPUs. This could be installed in slim rack cases, satisfying Criterion 2 regarding physical dimensions and weight. Such a cluster currently costs 12–15 k EUR, matching Criterion 3. We are also investigating the possibility to substitute the CPU cluster with Graphics Processing Units that would produce further reductions in size, weight and cost.

[22] AWA implemented on a system described above is planned for installation in Budapest, Hungary in the near future for testing and processing of archived data.

4. Summary

[23] The real-time monitoring of plasmaspheric electron densities cannot be achieved by human analysis of whistler events because of its labor intensive nature. The automation of the traditional whistler inversion method has proved to be impossible or at least unattainable at the moment. However, the application of a Virtual (Whistler) Trace Transformation leads to an algorithm that can be automated. We describe an implementation of AWA matching scientific, practical and economic criteria that is achievable on a PC cluster. The setup of such a system for test and archive data processing is under way. After successful testing of the AWA system, we plan to equip the AWDANet with similar systems. When this is achieved, AWDANet will be able to provide plasmaspheric density profiles for Space Weather related investigations and applications.

[24] **Acknowledgments.** This work was supported by the Hungarian Space Office.

[25] Robert Lysak thanks the reviewers for their assistance in evaluating this paper.

References

Bernard, L. C. (1973), A new nose extension method for whistlers, *J. Atmos. Terr. Phys.*, *35*, 871–880.

Carpenter, D. L. (1963), Whistler evidence of a "knee" in the magnetospheric ionization density profile, *J. Geophys. Res.*, *68*, 1675–1685.

Carpenter, D. L. (1988), Remote sensing of magnetospheric plasma by means of whistler mode signals, *Rev. Geophys.*, *26*, 535–549.

Carpenter, D. L., and R. R. Anderson (1992), An ISEE/whistler model of equatorial electron density in the magnetosphere, *J. Geophys. Res.*, *97*, 1097–1108.

Carpenter, D. L., B. L. Giles, C. R. Chappel, P. M. E. Décréau, R. R. Anderson, A. M. Persoon, A. J. Smith, Y. Corcuff, and P. Canu (1993), Plasmasphere dynamics in the duskside bulge region: A new look at an old topic, *J. Geophys. Res.*, *98*, 19,234–19,271.

Denton, R. E., J. Goldstein, and J. D. Menietti (2002), Field line dependence of magnetospheric electron density, *Geophys. Res. Lett.*, *29*(24), 2205, doi:10.1029/2002GL015963.

Ferencz, C., O. E. Ferencz, D. Hamar, and J. Lichtenberger (2001), *Whistler Phenomena—Short Impulse Propagation*, Kluwer Acad., Dordrecht, Netherlands.

Flandrin, P. (1999), *Time-Frequency/Time-Scale Analysis*, Academic, San Diego, Calif.

Hamar, D., C. Ferencz, J. Lichtenberger, G. Tarcsai, A. J. Smith, and K. H. Yearby (1992), Trace splitting of whistlers: a signature of fine structure or mode splitting in magnetospheric ducts?, *Radio Sci.*, *27*, 341–346.

Horne, R. B., and R. M. Thorne (2003), Relativistic electron acceleration and precipitation during resonant interactions with whistler-mode chorus, *Geophys. Res. Lett.*, *30*(10), 1527, doi:10.1029/2003GL016973.

Horne, R. B., R. M. Thorne, S. A. Galuert, N. P. Meredith, D. Pokhotelov, and O. Santolik (2007), Electron acceleration in the Van Allen radiation belts by fast magnetosonic waves, *Geophys. Res. Lett.*, *34*, L17107, doi:10.1029/2007GL030267.

Kodera, K., R. Gendrin, and C. D. Villedary (1976), A new method for the numerical analysis of non-stationary signals, *Phys. Earth Planet. Inter.*, *12*, 142–150.

Lichtenberger, J. (2009), A new whistler inversion method, *J. Geophys. Res.*, *114*, A07222, doi:10.1029/2008JA013799.

Lichtenberger, J., C. Ferencz, L. Bodnár, D. Hamar, and P. Steinbach (2008), Automatic whistler detector and analyzer system: Automatic whistler detector, *J. Geophys. Res.*, *113*, A12201, doi:10.1029/2008JA013467.

Meredith, N. P., R. B. Horne, S. A. Glauert, and R. R. Anderson (2007), Slot region electron loss timescales due to plasmaspheric hiss and lightning-generated whistlers, *J. Geophys. Res.*, *112*, A08214, doi:10.1029/2007JA012413.

Park, C. G. (1972), Methods to determine electron concentrations in the magnetosphere from nose whistlers, *Tech. Rep. 3454-1*, Radiosci. Lab., Stanford Electr. Lab., Stanford Univ., Stanford, Calif.

Park, C. G. (1974), Some features of plasma distributions in the plasmasphere deduced from antarctic whistlers, *J. Geophys. Res.*, *79*, 169–173.

Reeves, G. D. (1998), Relativistic electrons and magnetic storms: 1992-1995, *Geophys. Res. Lett.*, *25*, 1817–1820, doi:10.1029/98GL01398.

Rodger, C. J., J. Lichtenberger, G. McDowell, and N. R. Thomson (2009), Automatic whistler detection: Operational results from new zealand, *Radio Sci.*, *44*, RS2004, doi:10.1029/2008RS003957.

Sazhin, S. S., M. Hayakawa, and K. Bullough (1992), Whistler diagnostics of magnetospheric parameters: A review, *Ann. Geophys.*, *10*, 293–308.

Storey, L. R. O. (1953), An investigation of whistling atmospherics, *Philos. Trans. R. Soc. Ser. A*, *246*, 113–141.

Strangeways, H. J. (1982), The effect of multiduct structure on whistler-mode wave propagation, *J. Atmos. Terr. Phys.*, *44*, 901–912.

Tarcsai, G. (1975), Routine whistler analysis by means of accurate curve fitting, *J. Atmos. Terr. Phys.*, *37*, 1447–1457.

Tarcsai, G., P. Szemerédy, and L. Hegymegi (1988), Average electron density profiles in the plasmasphere between l = 1.4 and 3.2 deduced from whistlers, *J. Atmos. Terr. Phys.*, *50*, 607–611.

M. A. Clilverd, British Antarctic Survey, High Cross, Madingly Road, Cambridge CB3 0ET, UK. (macl@bas.ac.uk)

A. B. Collier, Hemanus Magnetic Observatory, PO Box 32, Hermanus 7200, South Africa. (collierab@gmail.com)

C. Ferencz, D. Hamar, and J. Lichtenberger, Space Research Group, Department of Geophysics and Space Sciences, Eötvös University, Pázmány P. Sétány 1/A, Budapest H-1117, Hungary. (spacerg@sas.elte.hu)

C. J. Rodger, Department of Physics, University of Otago, PO Box 56, Dunedin 9054, New Zealand. (crodger@physiscs.oatgo.ac.nz)

P. Steinbach, Research Group for Geology, Geophysics and Space Sciences, Hungarian Academy of Sciences, Pázmány P. Sétány 1/A, Budapest H-1117, Hungary. (spacerg@sas.elte.hu)